

A Multi-stage Cascaded Encoder-decoder Framework for CT-to-PET Image Conversion in Lung Imaging

Xiaoyu Deng¹, Kouki Nagamune^{1,2}, and Hiroki Takada¹

¹University of Fukui, 3-9-1 Bunkyo, Fukui, 910-0019, Japan

²University of Hyogo, 2167 Shosha, Himeji, Hyogo, 670-2280, Japan

Abstract

U-Net, a widely recognized deep learning architecture, excels in medical image processing tasks due to its symmetric encoder-decoder structure and skip connections, effectively preserving spatial information critical for precise segmentation. Although enlarging U-Net through depth increments, additional channels, improved skip connections, or integrating attention mechanisms such as Transformers can boost performance, it also introduces computational complexity and performance bottlenecks.

This study proposes a multi-stage cascaded framework utilizing sequentially connected simple encoder-decoder modules for the CT-to-PET medical image translation task, preserving simplicity within each encoder-decoder structure. The effectiveness of the framework is validated experimentally using publicly available lung cancer PET-CT datasets, assessing performance across various stages. Metrics including SSIM, PSNR, and MAE demonstrate significant improvements in image reconstruction quality, particularly at higher cascade stages, achieving peak SSIM of 0.9291 and PSNR of 28.8474 dB.

Visual comparison further indicates that despite high quantitative metric scores, certain visual artifacts remain due to transposed convolution operations, suggesting that pixel-level metrics alone may not comprehensively reflect perceptual quality. The proposed multi-stage cascaded U-Net model, therefore, presents strong potential for medical imaging applications, particularly in synthesizing high-quality PET images from CT scans, with recommendations for future integration of visual quality assessments and expert evaluations.

1 Introduce

U-Net is a deep learning architecture originally designed for segmentation tasks. Due to its outstanding performance and efficient structure, it has become highly popular in medical image processing. U-Net improves upon traditional convolutional neural networks (CNNs) through a symmetric "U"-shaped architecture, consisting of a contracting path (encoder) and an expansive path (decoder), also known as an encoder-decoder structure. A crucial feature of U-Net is its use of skip connections, which connect feature maps from the contracting path to corresponding layers in the expansive path. This design enables the network to leverage precise spatial information during upsampling, significantly enhancing the accuracy of segmentation boundaries, particularly important in medical imaging where structural delineation is critical.

Increasing the scale of U-Net models can involve deepening the network, increasing the number of feature map channels, improving skip connection structures, and incorporating attention modules like Transformers. While these enhancements can im-

prove performance, they also increase model complexity and computational demands, often leading to performance bottlenecks. In this research, multiple simple encoder-decoder structures are used to construct a generative network, verifying the performance of multi-stage models in medical image generation tasks.

The main contributions of this paper include proposing a multi-stage cascaded extension framework, constructing multiple multi-stage cascade models with simple encoder-decoder modules for CT-to-PET image conversion tasks, validating the effectiveness of this framework through experiments, and presenting performance metrics across various stages. The specific contributions are:

Proposing a multi-stage cascaded framework utilizing multiple simple encoder-decoder models for lung CT-to-PET image conversion tasks without altering individual encoder-decoder structures.

Experimentally validating the effectiveness of the proposed framework on publicly available paired PET-CT datasets, showcasing the performance of U-Net models at each stage, and monitoring various training and testing metrics.

Visually comparing images generated by different cascade models against real images to explore the effect of cascading on visual quality.

2 Related Works

Since the introduction of U-Net by Olaf et al. [1], it has been extensively employed due to its structural advantages and excellent performance in applications such as image denoising, medical image registration, and attenuation correction. It has also been applied in various other segmentation tasks including lesion segmentation and facial image restoration.

Armanious et al. [2] proposed an end-to-end GAN-based framework for medical image-to-image translation, demonstrating its performance in PET-CT translation, MR motion artifact correction, and PET denoising tasks. Singh et al. [3] presented a U-Net-based automated medical image registration method, employing GAN to generate pseudo-CT images from non-attenuation-corrected PET images, enhancing coronary angiography registration accuracy. Liu et al. [4] developed a method for generating pseudo-CT images for attenuation correction from single non-attenuation-corrected 18F-FDG PET images. Du et al. [5] reviewed six U-Net-based methods for medical image segmentation, including lung nodules, cardiac, and brain segmentation tasks. Zeng et al. [6] used a two-stage cascaded U-Net for facial image restoration, indicating potential advantages of multi-stage U-Net models for image generation tasks. Singh and Liu applied models with fine-tuned modules in medical image registration and attenuation correction, achieving notable results. While Armanious and Zeng utilized cascaded U-Net structures, multi-stage cascaded U-Net models for medical image generation remain underexplored. This study evaluates multi-stage cascaded U-Net models for CT-to-PET image conversion tasks using several metrics.

The Structural Similarity Index [7] (SSIM) measures structural similarity between two images, considering luminance, contrast, and structural information, ranging from -1 to 1, with 1 indicating identical images. The Multi-scale SSIM (MS-SSIM) extends SSIM across multiple scales, better assessing image quality across varying resolutions. Peak Signal-to-Noise Ratio [8] (PSNR) measures image reconstruction quality by comparing original and processed images, widely used in signal processing applications. Mean Absolute Error[9] (MAE) computes the average pixel intensity difference between reconstructed and original images, insensitive to outliers compared to Mean Squared Error (MSE), thus selected as an

evaluation metric given pixel scaling between 0 and 1 in PyTorch frameworks.

3 Method

The encoder-decoder architecture symmetrically captures context via a contracting path and achieves precise localization via an expansive path. This study constructs a standard U-Net convolutional neural network to convert CT images to PET images, optimized using a task-specific loss function.

The proposed cascaded framework comprises encoder, decoder, and visualization modules. The encoder extracts image features, the decoder reconstructs these features into output images, and the visualization module converts outputs into analyzable visual results. The detailed encoder-decoder structure is shown in Figure 1.

Encoder Block The encoder follows the typical architecture of a convolutional network. It consists of repeated application of two 3×3 convolutions, each followed by a rectified linear unit (ReLU) and a 2×2 max pooling operation [10] with stride 2 for down-sampling. At each downsampling step, the number of feature channels is doubled. The convolution operation in U-Net can be described by the following equation:

$$I' = \sum_{i,j} (I * K)(i, j) + b$$

where I represents the input image, K is the convolution kernel, b is the bias, and I' is the output feature map.

Decoder Block The decoder includes a series of upsampling and convolution operations. Each step in the expanding path includes an upsampling of the feature map followed by a 2×2 convolution that halves the number of feature channels, a concatenation with the correspondingly cropped feature map from the contracting path, and two 3×3 convolutions, each followed by a ReLU. Up sampling in the expanding path uses transposed convolutions to increase the size of the feature map:

$$U = K^T * I$$

where K^T is the transposed convolution kernel and U is the upsampled output.

Visual Block module, a variant decoder, converts output features from the decoder module into a visual format. Its structure is similar to a standard decoder but lacks skip connections and employs different non-linear functions, enhancing visual analysis.

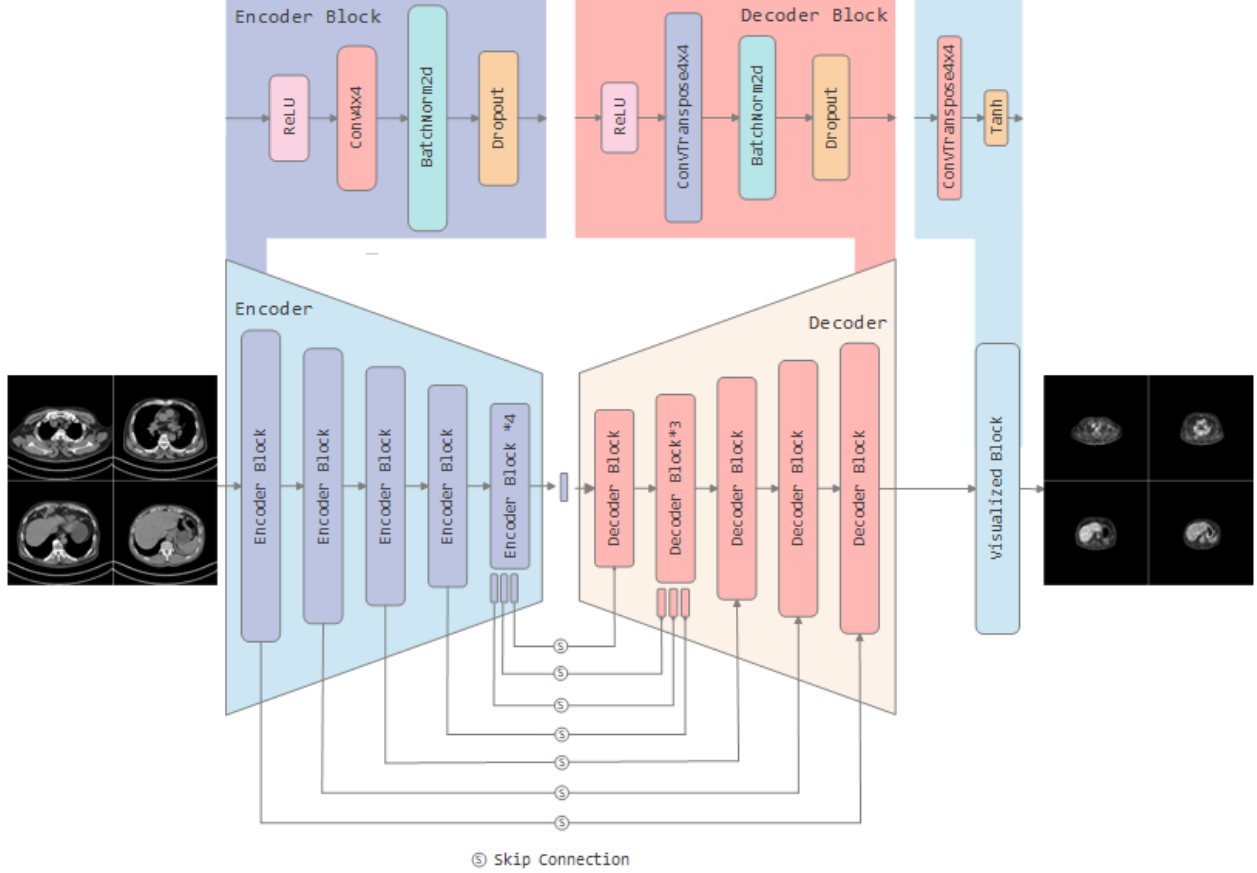


Figure 1: Schematic Diagram of Data Flow Within the Model. The PET image is shown on the left, and the CT image on the right. The blue modules correspond to the encoder architecture, while the orange modules represent the decoder architecture. The upper portion of the figure illustrates the fundamental structures of the encoder blocks, decoder blocks, and visualization blocks. The connections in the lower portion indicate the skip connections.

3.1 Cascaded Expansion Framework

This study introduces a cascaded expansion framework using multiple encoder-decoder structures cascaded sequentially. Each encoder-decoder output becomes the input for the subsequent stage, refining features progressively. This approach enhances model accuracy by capturing richer feature information at each stage. Although theoretically possible, segmented optimization strategies for different stages are not explored further here. Additionally, a Dual Stage Generator GAN (DSGGAN) with dense connections and segmented optimization mechanisms is introduced to capture stage-specific features more effectively. Table 2 details model parameter counts.

4 Experiments

This study employs the encoder-decoder architecture for cross-modality medical image conversion tasks, specifically to construct a U-Net that inputs a CT image and converts it into a corresponding PET image. In this research, the lung PET or CT scan data were powered by the National Cancer Institute Cancer Imaging Program (CIP) [12]. The dataset encompasses 251,135 lung scan images from 355 subjects, primarily collected between 2009 and 2011, including each subject’s gender, age, weight, smoking history, and cancer diagnosis classification. All scan data in the dataset are stored in DICOM format. This study processed these 251,135 scan data using the MicroDicom software on a Windows operating system. The subjects in the dataset are labeled according to the type of cancer: Type A for adenocarcinoma, Type B for small cell carcinoma, Type E for large cell carci-

Table 1: Encoder-decoder Setting Table

Block Name	input	output	trans	dropout
Encoder 1	3	16	-	-
Encoder 2	16	24	-	-
Encoder 3	24	42	-	-
Encoder 4	42	81	-	-
Encoder 5	81	114	-	-
Encoder 6	114	162	-	-
Encoder 7	162	162	-	-
Encoder 8	162	960	-	-
Decoder 1	960	960	162	0.5
Decoder 2	1122	162	162	0.5
Decoder 3	324	114	114	0.5
Decoder 4	228	81	81	-
Decoder 5	162	42	42	-
Decoder 6	84	24	24	-
Decoder 7	48	16	16	-
Visual Block	32	3	-	-

noma, and Type G for squamous cell carcinoma. Not all subjects’ data include both PET and CT scans. Therefore, this study selected imaging data from 38 confirmed Type B small cell carcinoma patients, including PET scans with CT scans, and fused enhanced images, resulting in 464 PET/CT pairs. Data was divided into training and testing sets, detailed in Table 3.

The optimization employed Mean Squared Error and adversarial loss functions [13], utilizing Adam optimizer [14] with a learning rate of 0.001 for gradual convergence. Optimal experimental results are listed in Table 4.

Metrics including SSIM, PSNR, and MSE were recorded over 200 training epochs, revealing high performance across training and testing datasets. Stage07 and Stage10 models exhibited higher SSIM and PSNR values, indicating superior reconstruction quality.

Figure 2 illustrates SSIM rapidly increasing in initial training (first 25 epochs), stabilizing around 0.9. DSGGAN exhibited fluctuations possibly due to overemphasis on high-dimensional features, but overall SSIM remained high.

PSNR (Figure 3) showed rapid initial improvements with subsequent fluctuations, particularly in 8-, 6-, 4-, and 3-stage models, indicating potential generalization issues with complex data or smaller datasets. Overall, PSNR remained consistently good.

The MAE curve in Figure 4 declines steeply at the beginning of training, indicating rapid parameter adaptation. Nevertheless, all models converge to uniformly low MAE scores for two principal reasons: (i)

Table 2: Parameters of Neural Networks.

Architectures	Parameters
U-Net[1]	54.41
Cas-UNet[6]	108.82
DualStageGGAN[11]	92.54
Stage01	22.13
Stage02	44.26
Stage03	66.39
Stage04	88.52
Stage05	110.65
Stage06	132.77
Stage07	154.90
Stage08	177.03
Stage09	199.16
Stage10	221.29

The table depicts the Parameters of different generators. The quantity of parameters is expressed in millions.

Table 3: Dataset Partition of Experiment

Params count	Test	Train	Total
Lung PET/CT Pair	64	400	464
Total Images	128	800	928

the PET intensities are normalized to the [0,1] range, and (ii) dark pixels constitute the majority of each image. Consequently, a well-trained network quickly discovers that synthesizing images with a disproportionately large share of near-black pixels is an efficient way to minimize the MAE objective. Despite these encouraging numbers, a lower MAE does not necessarily translate into superior perceptual quality. Hence, complementary visual-comparison experiments are required, as purely numerical metrics provide an incomplete—and potentially misleading—assessment of image fidelity.

Visual comparisons (Figure 5) indicated pixel-level metrics differed from perceived quality, highlighting artifacts in certain stages due to transpose convolutions. Quantitative metrics did not fully reflect visual quality, underscoring the need for expert evaluations or prior knowledge. Although the Stage10 and DSGGAN models attained excellent quantitative scores, the images they produced were noticeably blurred. DSGGAN, in particular, exhibited strong numerical performance yet fell short in visual fidelity—a deficiency that may arise from its distinctive skip-connection design, which can overfit when confronted with complex data or limited sample sizes. These results underscore that pixel-level metrics alone cannot fully capture perceptual quality; a

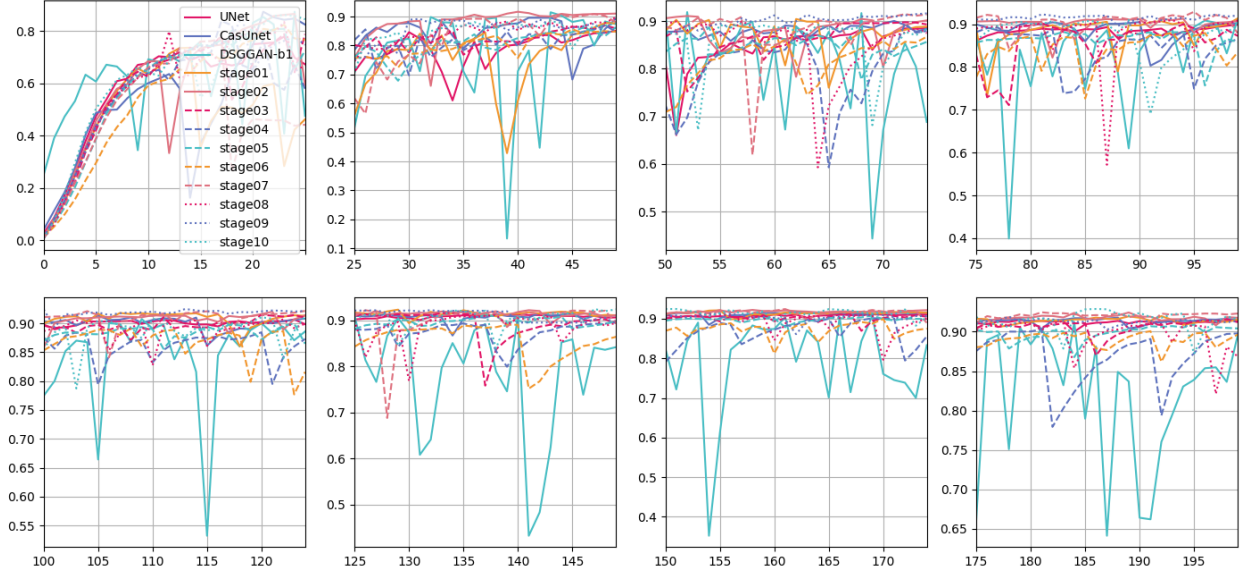


Figure 2: SSIM Line Figure of All Epoch in Test Process

Table 4: Max SSIM,PSNR,MAE Results of Experiment

Stage Count	SSIM	PSNR	MAE
U-Net	0.9149	27.7411	0.0119
Cas-Unet	0.9182	27.9950	0.0109
DSGGAN	0.9122	28.7630	0.0106
1 Stages	0.9006	28.3584	0.0119
2 Stages	0.9122	28.5897	0.0110
3 Stages	0.9030	28.7249	0.0105
4 Stages	0.9160	28.1237	0.0110
5 Stages	0.9243	28.1736	0.0111
6 Stages	0.9237	28.1355	0.0105
7 Stages	0.9291	28.2716	0.0103
8 Stages	0.9134	28.4860	0.0119
9 Stages	0.9248	28.4371	0.0108
10 Stages	0.9288	28.8474	0.0103

more comprehensive evaluation that integrates expert judgment or domain-specific priors is therefore essential. By contrast, the Stage07 network delivered competitive quantitative results while producing images of comparatively higher visual quality. Overall, our proposed frameworks indicate that cascade-based extensions can achieve robust performance in medical image synthesis, but they also reveal intrinsic limitations that warrant further investigation.

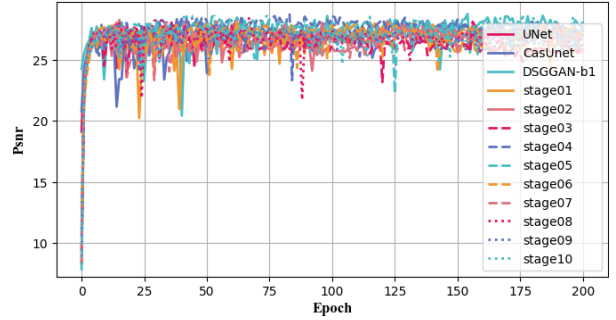


Figure 3: PSNR Line Figure of All Epoch in Test Process

5 Conclusion

The proposed cascaded framework effectively enhanced performance and demonstrated stability. Future studies should integrate visual quality assessments and expert evaluations to increase practical utility in medical image translation tasks. The study’s findings suggest that the multi-stage cascaded U-Net model can be a valuable tool for medical image synthesis, with potential applications in various medical imaging tasks. The results indicate that the model can effectively learn to generate high-quality images from CT scans, which could aid in improving diagnostic accuracy and treatment planning in clinical settings. Further research is needed to explore the model’s performance on larger datasets and its

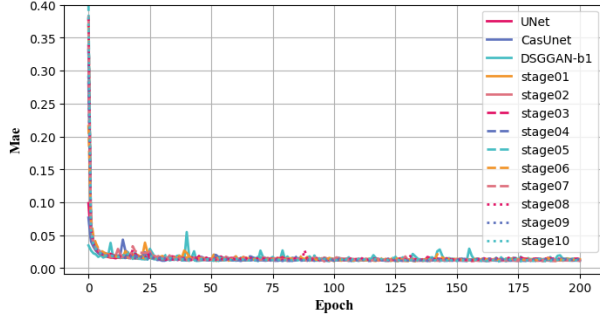


Figure 4: MAE Line Figure of All Epoch in Train and Test Process

applicability to other imaging modalities.

Acknowledage

We would like to express our sincere gratitude to the National Cancer Institute Cancer Imaging Program for generously making their high-quality medical imaging dataset available and authorized for use on the Internet, providing indispensable resources for the smooth conduct of this research.

References

- [1] Olaf Ronneberger, Philipp Fischer, and Thomas Brox. U-Net: Convolutional Networks for Biomedical Image Segmentation. In Nassir Navab, Joachim Hornegger, William M. Wells, and Alejandro F. Frangi, editors, *Medical Image Computing and Computer-Assisted Intervention – MICCAI 2015*, volume 9351, pages 234–241. Springer International Publishing, Cham, 2015. Series Title: Lecture Notes in Computer Science.
- [2] Karim Armanious, Chenming Jiang, Marc Fischer, Thomas Küstner, Tobias Hepp, Konstantin Nikolaou, Sergios Gatidis, and Bin Yang. MedGAN: Medical image translation using GANs. *Computerized Medical Imaging and Graphics*, 79:101684, January 2020.
- [3] Ananya Singh, Jacek Kwiecinski, Sebastien Cadet, Aditya Killekar, Evangelos Tzolos, Michelle C Williams, Marc R. Dweck, David E. Newby, Damini Dey, and Piotr J. Slomka. Automated nonlinear registration of coronary PET to CT angiography using pseudo-CT generated from PET with generative adversarial networks. *Journal of Nuclear Cardiology*, 30(2):604–615, April 2023.
- [4] Fang Liu, Hyungseok Jang, Richard Kijowski, Gengyan Zhao, Tyler Bradshaw, and Alan B. McMillan. A deep learning approach for 18F-FDG PET attenuation correction. *EJNMMI Physics*, 5(1):24, December 2018.
- [5] Getao Du, Xu Cao, Jimin Liang, Xueli Chen, and Yonghua Zhan. Medical Image Segmentation based on U-Net: A Review. *Journal of Imaging Science and Technology*, 64(2):020508–1–020508–12, March 2020.
- [6] Chengbin Zeng, Yi Liu, and Chunli Song. Swin-CasUNet: Cascaded U-Net with Swin Transformer for Masked Face Restoration. In *2022 26th International Conference on Pattern Recognition (ICPR)*, pages 386–392, Montreal, QC, Canada, August 2022. IEEE.
- [7] Zhou Wang, A.C. Bovik, H.R. Sheikh, and E.P. Simoncelli. Image quality assessment: from error visibility to structural similarity. *IEEE Transactions on Image Processing*, 13(4):600–612, April 2004.
- [8] Alain Hore and Djemel Ziou. Image Quality Metrics: PSNR vs. SSIM. In *2010 20th International Conference on Pattern Recognition*, pages 2366–2369, Istanbul, Turkey, August 2010. IEEE.
- [9] T. Chai and R. R. Draxler. Root mean square error (RMSE) or mean absolute error (MAE)? – Arguments against avoiding RMSE in the literature. *Geoscientific Model Development*, 7(3):1247–1250, June 2014.
- [10] Naila Murray and Florent Perronnin. Generalized Max Pooling. In *2014 IEEE Conference on Computer Vision and Pattern Recognition*, pages 2473–2480, Columbus, OH, USA, June 2014. IEEE.
- [11] Huabin Wang, Xiangdong Wang, Fei Liu, Grace Zhang, Gong Zhang, Qiang Zhang, and Michael L. Lang. DSG-GAN: A dual-stage-generator-based GAN for cross-modality synthesis from PET to CT. *Computers in Biology and Medicine*, 172:108296, April 2024.
- [12] Ping Li, Shuo Wang, Tang Li, Jingfeng Lu, Yunxin HuangFu, and Dongxue Wang. A Large-Scale CT and PET/CT Dataset for Lung Cancer Diagnosis, 2020.
- [13] Zhaoqing Pan, Weijie Yu, Bosi Wang, Haoran Xie, Victor S. Sheng, Jianjun Lei, and Sam

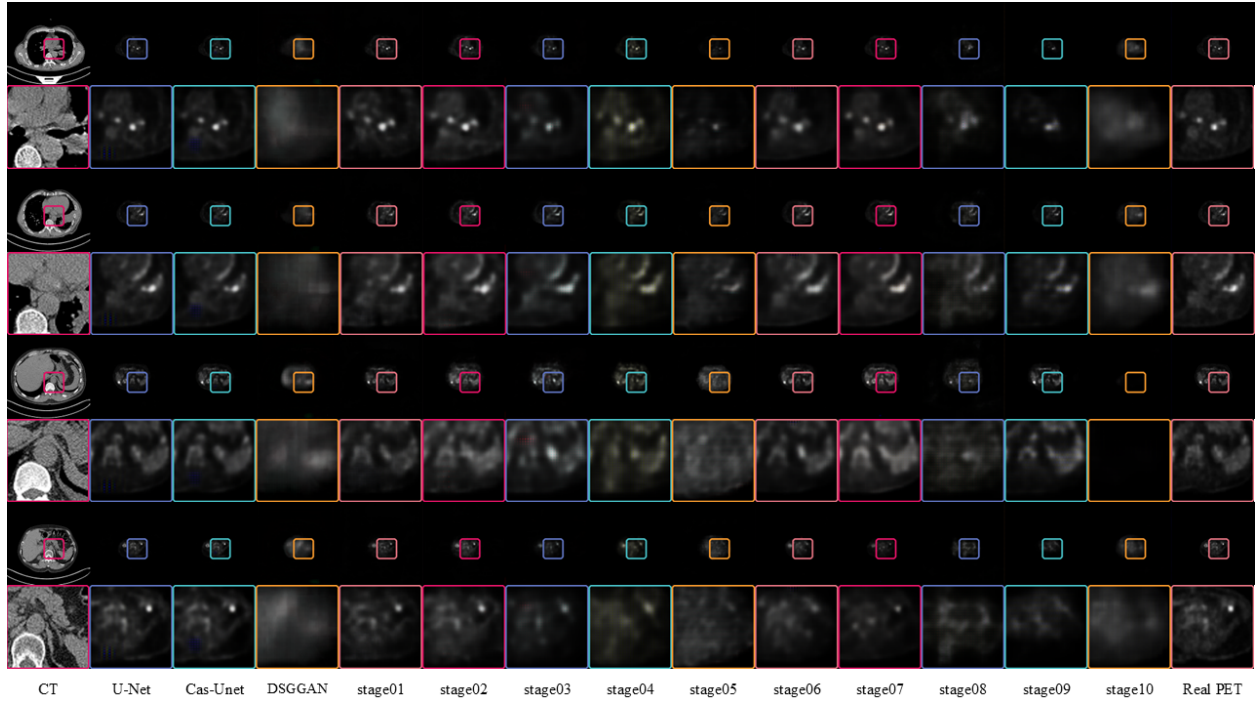


Figure 5: The figure displayed here showcases PET images generated by various models, compared alongside real CT and PET images. The odd rows present the complete paired PET-CT images, while the even rows provide magnified views of specific regions within these pairs. Each model utilizes the CT image located at the extreme left as the input. The real PET images positioned at the extreme right serve as references for comparison.

Kwong. Loss Functions of Generative Adversarial Networks (GANs): Opportunities and Challenges. *IEEE Transactions on Emerging Topics in Computational Intelligence*, 4(4):500–522, August 2020.

- [14] Zijun Zhang. Improved Adam Optimizer for Deep Neural Networks. In *2018 IEEE/ACM 26th International Symposium on Quality of Service (IWQoS)*, pages 1–2, Banff, AB, Canada, June 2018. IEEE.